energies

MDPI

Article

Numerical Investigation and Simulation of Hydrogen Blending into Natural Gas Combustion

Laura Jung [1,2,*], Alexander Mages [1,2] and Alexander Sauer [1,2]

[1] Institute for Energy Efficiency in Production EEP, University of Stuttgart, 70569 Stuttgart, Germany
[2] Fraunhofer Institute for Manufacturing Engineering and Automation IPA, 70569 Stuttgart, Germany
* Correspondence: laura.jung@ipa.fraunhofer.de

Abstract: This study reviews existing simulation models and describes a selected model for analysing combustion dynamics in hydrogen and natural gas mixtures, specifically within non-ferrous melting furnaces. The primary objectives are to compare the combustion characteristics of these two energy carriers and assess the impact of hydrogen integration on furnace operation and efficiency. Using computational fluid dynamics (CFD) simulations, incorporating actual furnace geometries and a detailed combustion and NOx emission prediction model, this research aims to accurately quantify the effects of hydrogen blending. Experimental tests on furnaces using only natural gas confirmed the validity of these simulations. By providing precise predictions for temperature distribution and NOx emissions, this approach reduces the need for extensive laboratory testing, facilitates broader exploration of design modifications, accelerates the design process, and ultimately lowers product development costs.

Keywords: hydrogen blending; numerical simulation; CFD; combustion; furnace; melting

Citation: Jung, L.; Mages, A.; Sauer, A. Numerical Investigation and Simulation of Hydrogen Blending into Natural Gas Combustion. *Energies* **2024**, *17*, 3819. https://doi.org/10.3390/en17153819

Academic Editors: Daniela Anna Misul and Simone Salvadori

Received: 6 July 2024
Revised: 20 July 2024
Accepted: 27 July 2024
Published: 2 August 2024

1. Motivation

Germany is committed to reducing greenhouse gas emissions by at least 65% from 1990 levels by 2030, with an ambitious target of an 88% reduction by 2040 [1]. Approximately 67% of the final energy consumption in Germany is dedicated to producing process heat, with high-temperature industrial processes (over 100 °C) accounting for 91.2% of this demand [2] (pp. 16–20), [3] (pp. 11–14). These processes, prevalent in the metals industry, melting and casting, glass production, paper production, and food processing, heavily depend on fossil fuel combustion, significantly contributing to greenhouse gas emissions.

To mitigate these emissions, hydrogen can be blended into current technologies as an interim solution. Hydrogen is classified as "green", emission-free, and climate-neutral only if it is produced using electricity from 100% renewable sources, such as solar or wind power. Another emission-free option is "orange" hydrogen, which is derived from organic materials such as agricultural, forestry, household, and industrial waste [4,5] (pp. 71–75). Hydrogen can be utilised in a wide range of high-temperature industrial applications, with molten carbonate fuel cells (MCFC) and solid oxide fuel cells (SOFC) using hydrogen to achieve temperatures between 450 °C and 1000 °C [6]. Furthermore, hydrogen combustion can be adapted to existing natural gas burner technology, making it a versatile option for emission reduction.

Despite its potential, hydrogen's current availability and high-cost pose challenges. Thus, blending hydrogen with natural gas in existing technologies offers a practical approach to reducing emissions while maintaining operational efficiency. This strategy not only leverages existing infrastructure but also provides a scalable pathway to integrate higher proportions of green hydrogen as its availability increases and costs decrease.

This article explores the dynamics of hydrogen and natural gas mixtures in high-temperature processes, specifically in the melting of non-ferrous materials. It begins with

an overview of the current operating modes and technologies used in melting furnaces. Following this, the combustion characteristics and the changes resulting from hydrogen integration are presented. To analyse the impact of hydrogen blending on existing burner technologies used in gas-fired furnaces within the die-casting of non-ferrous metals, a detailed simulation model is introduced. This simulation approach is applied to a specific furnace geometry (the crucible furnace) representative of industrial settings, investigating the changes in temperature distribution and emissions at varying percentages of hydrogen blended into natural gas.

2. Operating Modes of Furnaces for the Die-Casting of Non-Ferrous Metals

Non-ferrous metal casting primarily involves aluminium and magnesium alloys within the light metal category and copper and zinc alloys within the heavy metal category. This process begins by preheating and melting these metals in a furnace. The molten metal is injected under high pressure into a mould cavity to achieve the desired shape. Various types of furnaces are utilized in non-ferrous metal casting, including crucible furnaces, shaft melting furnaces, hearth- and bath-type furnaces, and twin-chamber melting furnaces. The crucible furnace offers significant flexibility as the crucible can be replaced to accommodate different alloys. This furnace type benefits from low burnup since the melt only contacts air through indirect heating [7]. The melting process in these furnaces is energy-intensive, with different systems providing the necessary melting power:

- Electric crucible furnaces have the advantage of higher durability of the crucible and lower emissions. However, they come with high investment and operational costs due to the use of electrical energy [8].
- Gas-fired furnaces utilize the combustion of natural gas or fossil fuels to melt metals. The emissions from fossil fuel combustion can be significantly higher than the electrical-driven melting process. The furnaces utilize burners to supply, mix, and burn air and fuel. The design of the burner influences the burning rate, flame front, and flame length. Industrial burners are classified into four categories [9]:
    - Cold Air Burners: Draw air directly from the ambient environment.
    - Hot Air Burners: Use external heat exchangers to preheat the air.
    - Self-Recuperative Burners: Recover waste heat from exhaust gases to preheat the incoming combustion air, improving energy efficiency.
    - Regenerative Burners: Capture waste heat from combustion and store it in a regenerator heat exchanger.

Cold air jet burners with a mixing head are most commonly used in non-ferrous heat treatment furnaces and non-ferrous melting furnaces [9,10]

- Hybrid furnaces can switch between energy sources, allowing peak loads to be covered with the other energy source. Integration with the energy exchange market provides cost savings, and bonuses for regulating energy demand could also be profitable. This approach is currently being tested in a prototype [11,12].

3. Hydrogen Combustion

3.1. Challenges of Hydrogen Combustion Compared to Natural Gas

Natural gas (methane) is typically used as the energy source for gas-fired furnaces in the die-casting of non-ferrous metals. The different physical properties of hydrogen and natural gas present challenges for the integration of hydrogen during combustion. Hydrogen has a lower density and energy density per volume than natural gas, necessitating a higher volume of hydrogen to supply the same amount of energy as methane. The flammability range is 4–75 vol%, allowing for a broader range of air/fuel ratios. This can be advantageous, enabling hydrogen to run on lean mixtures and, thus, improve fuel efficiency. Further, hydrogen can burn in lean blends because it requires lower ignition energy (0.02 mJ). However, this low ignition energy can also pose problems, as hot spots can become ignition sources. Hydrogen has a lower heating value of 120 MJ/kg (net calorific

value), which is higher than methane, resulting in more heat release during combustion. Table 1 shows the properties of hydrogen compared to methane.

Table 1. Properties of hydrogen compared to methane [13–15].

Property	Hydrogen H_2	Methane CH_4	Units
Molecular weight	2.02	16.04	[g/mol]
Density (gaseous)	0.084	0.668	$[kg/m^3]$
Density (liquefied)	71	430–470	$[kg/m^3]$
Energy density (gaseous)	3	12.6	$[MJ/dm^3]$
Flammability range in Air	4–75	5–15	[vol%]
Stoichiometric air/fuel ratio	34.2	17.1	$[kg_{air}/kg_{fuel}]$
Flammability limits (λ)	0.14–10	0.6–2	[-]
Minimum ignition energy	0.02	0.29	[mJ]
Auto ignition temp. in air	858	810	[°K]
Laminar flame velocity	230–320	38–42	[cm/s]
Lower heating value	120	50	[MJ/kg]
Adiabatic flame temperature (air)	2483	2236	[°K]

3.2. Hydrogen Chemical Kinetics

Hydrogen combustion typically involves the reaction of hydrogen (H_2) with air (O_2, N_2) to produce water (H_2O) and nitrogen (N_2). This process can be summarized by a single global reaction in chemical kinetics (Equation (1)) [16].

$$2H_2 + (O_2 + 3.7N_2) \rightarrow 2H_2O + 3.7N_2 \quad (1)$$

However, particularly when hydrogen reacts with air, numerous intermediate reactions occur before the final products, water and nitrogen, are formed. These intermediate steps are detailed in [17], providing an overview of the 126 possible intermediate reactions during hydrogen combustion. A critical aspect to consider during hydrogen combustion is the emissions produced, which must be controlled to meet environmental regulations. Nitrous oxide (N_2O) and nitrogen dioxide (NO_2) are key NO_x contributors, with multiple intermediate reactions governing their formation and decomposition. Further, the formation of NO involves various reactions, significantly influenced by high temperatures.

To represent these complex mechanisms, various reaction mechanisms have been validated to accurately depict the chemical kinetics of hydrogen combustion. Advancements in technology and experimental methods have led to an accurate representation of combustion, enabling the prediction of the chemical kinetics and combustion characteristics of hydrogen. Table 2 provides an overview of the different mechanisms used to model combustion, detailing the involved species or chemical entities and the reactions within the proposed mechanisms.

Table 2. Models for reaction mechanisms for hydrogen combustion [16].

Mechanism	Fuels	Species	Reactions	References
GRI Mech 3.0	Hydrogen and Natural Gas	53	325	[18]
San Diego	Hydrogen and Methane	57	268	[19]
Crek Modeling Group	Hydrogen	21	62	[20–22]
Explosion dynamics laboratory	Hydrogen	14	42	[23]

3.3. Hydrogen Blends

The infrastructure for hydrogen blends in gas networks has been adapted, and a blend of up to 20 Vol-% H_2 has already been achieved. A higher volume of 30 Vol-% is expected within the next years [24]. Blending hydrogen into natural gas pipelines presents a promising method to enhance hydrogen transport using existing infrastructure, eliminating

the need for entirely new pipeline systems [25]. Hydrogen's lower volumetric energy density compared with natural gas can be challenging because higher operating pressures are required to maintain the same transmission capacity [26]. In addition, the different material properties can affect the combustion characteristics [27].

Lee et al. [13] conducted an experimental investigation on hydrogen blends in a constant-volume chamber. The results indicate that higher hydrogen fractions in the fuel significantly enhance heat release rates, combustion pressure, and burning velocity. Increasing the hydrogen fraction in the fuel blend reduces hydrocarbons (HC) and carbon dioxide (CO_2) emissions, benefiting emission regulations, but increasing nitrogen oxide (NO_x) emissions. Further studies by Ozturk et al. [28] showed that a 0.3 hydrogen blending ratio improved energy efficiency by 4.4% and reduced CO_2 emissions by 20.87%, though NO_x emissions fluctuated with different hydrogen blends.

This paper aims to investigate the blending of hydrogen into the furnaces used in die-casting. The following sections present the background of computational fluid dynamics (CFD) simulations and the CFD model to study the effect of blending hydrogen into the burner of a melting furnace.

4. Computational Fluid Dynamics (CFD) for Hydrogen and Hydrogen Blends Flames

CFD simulates fluid flow and heat transfer processes through the numerical solution of equations. These simulations are based on fluid mechanics, which relies on differential equations. The mathematical foundation for describing flow processes is provided by the three-dimensional conservation laws of mass, momentum, and energy [29].

Turbulent flow simulations commonly employ Reynolds-Averaged Navier–Stokes (RANS) models due to their balance between computational efficiency and accuracy. The RANS equations are derived from the Navier–Stokes equations by decomposing the flow variables into mean and fluctuating components. These turbulence models describe the turbulent viscosity using the turbulent kinetic energy (k) and dissipation rate (ε). CFD programs offer various turbulence models based on the k-ε model and other parameters, which help stabilize the solution [26]. In turbulent flows, large velocity gradients exist near the wall, where no-slip conditions reduce the flow velocity to zero. Wall models resolve these conditions in the viscous sublayer near the wall. The logarithmic wall law is typically employed for the wall-near region, representing the transition between low and high flow velocities and Reynolds numbers [30].

The finite volume method is the most widely used numerical approach in CFD. The computational domain is discretized into finite volumes in this method, using a numerical grid. Meshes composed of polyhedra can easily represent complex geometries with local refinements. After discretizing, the differential equations are solved iteratively by applying known boundary conditions. The numerical solution must be checked for consistency and convergence. A method is considered consistent if the discretization error approaches zero as the grid is refined indefinitely. A solution is said to converge if it tends towards the exact solution, which can be verified using residuals [31,32].

4.1. State of the Art for Numerical Investigation of Hydrogen and Hydrogen Blends Flames

A comprehensive literature review was conducted to identify publications focused on the numerical modelling of methane, hydrogen, or blend flames in jet and swirl burners. The selected publications, summarized in Table 3, effectively employ numerical methods to characterize the combustion properties of various hydrogen blends. These studies also validate their simulation results against experimental data, enabling an accurate assessment of the selected combustion and turbulence models. An overview of these findings is provided in Table 3.

Table 3. Literature review on numerical investigations for jet and swirl burners.

Publication	Burner	Combustion Modell	Turbulence Model	H_2–Blending
Bouziane et al. [33]	Swirl	Eddy Dissipation	RNG k-ε model	40 and 80%
Capurso et al. [34]	Swirl	Flamelet model	Realizable k-ε	30%
Cellek et al. [35]	Swirl	Eddy Dissipation	Realizable k-ε	25, 50, and 75%
Ilbas et al. [36,37]	Jet	Arrhenius kinetic rate and the eddy break-up model	Standard k-ε model	10 and 70%
Pashchenko [38]	Swirl	Finite-Rate	RNG k-ε turbulence	40 and 80%
Stefanizzi et al. [39]	Swirl	Flamelet model	Reynolds Stress Model	30%
Ziani et al. [40]	Jet	Flamelet model	Modified k-ε model	0 to 50%

As shown in Table 3, Reynolds-Averaged Navier–Stokes (RANS) models are commonly used with various turbulence and combustion models for these simulations. Ilbas et al. [36] investigated several turbulence models and found that the standard k-ε model delivered the most accurate results. Similarly, Ziani et al. [40] explored various turbulence models and concluded that the modified k-ε model provided the closest agreement with experimental data.

Simulating a chemically reacting system involves formulating and solving additional transport equations for species concentrations or mixture fractions. Various approaches are employed for combustion simulations. Ilbas et al. [36] utilize the Arrhenius kinetic rate and the eddy break-up model to calculate reaction rates in turbulent flow. Cellek et al. [35] and Bouziane et al. [33] apply the Eddy Dissipation combustion model. Ziani et al. [40], Stefanizzi et al. [39], and Capurso et al. [34] employ the flamelet model for non-premixed turbulent combustion.

Bouziane et al. [33] show that flame mixture structures and shapes can be predicted using combustion models, comparing them against experimental data, with temperature profiles exhibiting different trends among fuel mixtures. Cellek et al. [35] investigate hydrogen blend combustion in an industrial low-swirl burner-boiler system, quantifying increased NO_x emissions, reduced CO emissions, and lower fuel consumption with higher hydrogen blends. Ilbas et al. focus on combustion characteristics and pollutant formation, revealing that air staging reduces NO_x emissions by approximately 20% in an axisymmetric small burner [36] and a model combustor with turbulent non-premixed hydrogen diffusion flames [37]. Pashchenko [38] models synthetic fuel combustion in a swirling flame, varying the molar fraction of hydrogen and comparing numerical and experimental data regarding flame contours, temperature, and NO_x emissions. Stefanizzi et al. [39] analyse hydrogen-enriched fuel behaviour in combustion processes using a laboratory-scale swirl premix burner, validating the model against experimental data through cold flow partially premixed combustion numerical simulation. Ziani et al. [40] conducted numerical investigations on hydrogen–methane mixtures, observing an increase in combustion temperature and a decrease in CO and CO_2 mass fractions.

4.2. Combustion Model

The flamelet model was chosen for simulating non-premixed turbulent hydrogen mixture combustion due to its accuracy in predicting combustion chemistry and its compatibility with advanced turbulence models. Flamelet models simulate diffusion flames and assume fast chemical reactions to simplify the combustion into a mixing problem. In industrial furnaces, fuel and air are typically fed separately into the combustion chamber, where mixing occurs before combustion. This fuel-air mixing is driven by turbulent diffusion processes, resulting in diffusion flames. The theoretical description of diffusion flames often assumes fast chemical reactions, where chemical reactions are much faster than diffusion. Therefore, diffusion and mixing determine the combustion time rate. Under this assumption, important global properties of diffusion flames can be described, allowing for the simplification of chemical kinetics [41] (pp. 156–170).

Flamelet models use the mixture fraction, ranging from 0 (unburned) to 1 (burned), to represent combustion. The mixture fraction f is defined as the mass fraction of fuel in the mixture, where index 1 defines the fuel gas mass flow $\dot{m}_1$, and index 2 defines the oxidizer mass flow $\dot{m}_2$. Based on the resulting mass fraction profiles of $\dot{m}_1$ and $\dot{m}_2$, the flamelet model represents temperature and concentration as a function of mixing fraction f (Equation (2)). An additional variable, the diffusion rate parameter χ, is considered in this model, defined with the thermal diffusivity D and the mixture fraction f (Equation (3)). The diffusion rate can be understood as the reciprocal of the characteristic time of diffusion or dwell time [41] (pp. 156–170).

Mixture Fracture:

$$f = \frac{\dot{m}_1}{\dot{m}_1 + \dot{m}_2} \tag{2}$$

Scalar Dissipation:

$$\chi = 2D|\nabla f|^2 \left[\frac{1}{s}\right] \tag{3}$$

The interaction of turbulence and chemistry is considered with an assumed probability density function (PDF). It describes the relationships between the mixture fraction and species fractions, density, and temperature. The probability density function $p(f)$ is the time fraction the fluid spends in the state f [30]. Figure 1 describes the PDF function: On the right side, the time history of the mixture fraction at a point in the flow is shown, which fluctuates around the mean value. Further, the probability density function as a function of f is displayed on the left side.

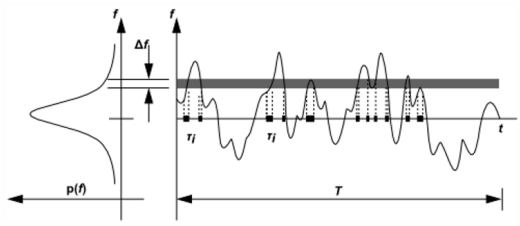

Figure 1. Graphical description of the probability density function [30].

The function $p(f)$ is unknown. CFD programs model the PDF $p(f)$ as a mathematical function approximating the experimentally observed PDF shapes. The assumed shape of the PDF is described by two parameters [30]:

- The mean mixture fraction $\overline{f}$
- The mean mixture variance $\overline{(f'^2)}$

4.3. Model for NO_x Formation

NO_x emissions, primarily comprising nitric oxide (NO), nitrogen dioxide (NO_2), and nitrous oxide (N_2O), need special consideration in combustion modelling. The non-premixed flamelet model (Section 4.2) assumes rapid chemical reactions to simulate flames and combustion processes. However, pollutants like NO_x form through slower chemical reactions, which the non-premixed combustion model does not simulate effectively. CFD programs incorporate a NO_x post-processing model that utilizes combustion results as input and equations during a post-simulation to enhance emission accuracy. To predict NO_x emissions, further mass transport equations for NO species are solved, considering convection, diffusion, production, and consumption of NO. The CFD NO_x process can model thermal, prompt, and intermediate NO_x formation [30]:

- Thermal NO_x formation occurs through the oxidation of atmospheric nitrogen within the combustion air. This process is governed by a series of temperature-dependent chemical reactions collectively called the extended Zeldovich mechanism.

- Prompt NO_x is generated at the flame front through rapid reactions and typically occurs in combustion environments with short residence times, and the conditions are either low-temperature or rich in fuel.
- The formation of NO_x from intermediate N_2O represents a significant pathway, contributing up to 90% of NO_x produced during combustion. Under conditions of high pressure and high oxygen concentration, NO_x formation is promoted. When fuel and oxygen are substantially diluted with inert gases like nitrogen, the combustion reactions and the associated heat release occur predominantly in the diffuse zone [42] (pp. 591–610).

For non-premixed combustion using the flamelet model, the PDF function and turbulence model derived from combustion data can be employed to simulate fluctuations in temperature and species concentrations. These fluctuations significantly affect the flame's characteristics and NO_x formation. This approach facilitates the incorporation of the effects of turbulence and mixture fraction variance into the calculation of NO_x emissions.

5. CFD Simulation Model Setup

The numerical simulation of the crucible furnace used in the die-casting was modelled with Ansys® Fluent [43], a CFD simulation tool that allows users to mesh and parameterize the solver using a single program. To set the simulation, the Ansys Theory Guide [30] and Users Guide [44] were used to meet the requirements of the CFD program.

5.1. Model Setup and Meshing

For the simulation, a model of a crucible furnace in the magnesium die-casting industry was used. The geometry model comprises a cold air jet burner, air and fuel gas inlet channels, a combustion chamber, and the crucible wall furnace. Figure 2 shows the geometry model and measures. The model has been simplified with Ansys SpaceClaim [45] for simulation purposes. The crucible furnace has a diameter of 520 mm and a length of 590 mm. Additionally, the inlet, which includes the burner and the combustion chamber, has a length of approximately 510 mm. The length of the burner is around 300 mm. The axis of the burner is not positioned at the centre of the crucible; rather, it is located tangentially to the crucible's edge, as shown in Figure 2 (right). The choice of burner position reflects the specific requirements, with the geometry carefully considered in consultation with the furnace manufacturer.

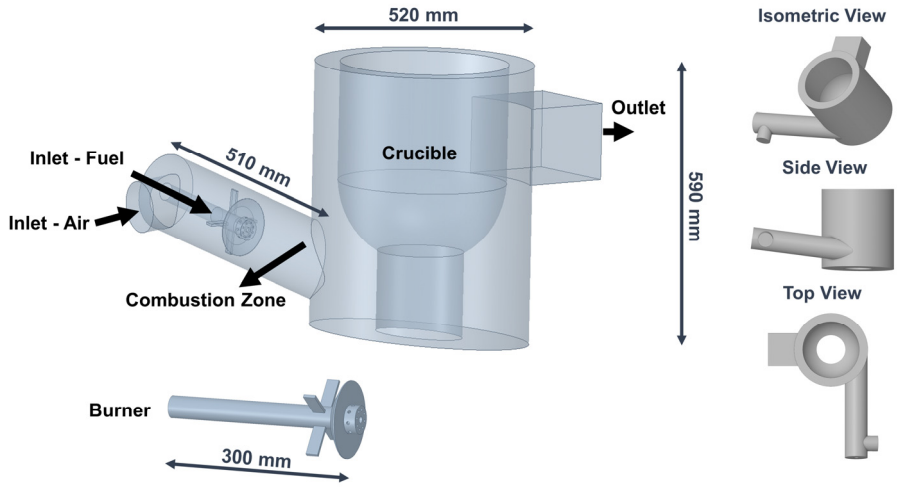

Figure 2. Furnace geometry model used within the CFD simulation.

The first step is to generate an unstructured mesh that accurately represents the geometry. This mesh serves as the discretized domain for the simulation and is the basis for solving the fluid flow equations. Ansys Fluent Meshing [43] was used for the meshing process. The meshing tool automatically divides the entire model into polyhedral meshes

of approximately 4 mm and employs a block-structured approach for the boundary layers. The mesh comprises 7.6 million cells and 25 million nodes. Element quality metrics include an average skewness of 0.56 and a minimum orthogonal quality of 0.15. Local refinement was applied uniformly to the combustion and inlet areas, with a cell size of 3 mm, where significant flow changes are expected. Ansys Fluent also provides a mesh improvement feature that automatically remeshes cells with poor quality. To ensure the proper resolution of the near-wall flow, 25 layers have been selected that continuously increase in size normal to the wall. Figure 3 illustrates the grid model used for the calculation in the furnaces.

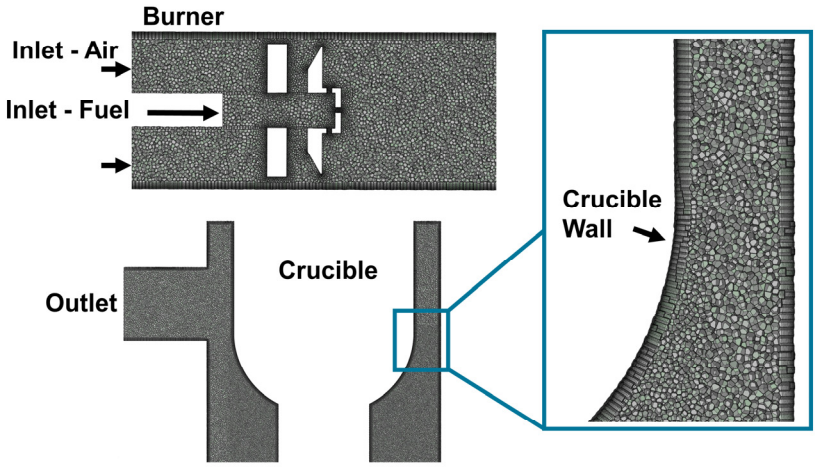

Figure 3. Furnace geometry meshing.

5.2. Solver Settings

The solver setting is pressure-based and steady-state. The results of a steady-state calculation assume that the system is in equilibrium and does not change with time. The energy equation is enabled to include the effect of heat losses on the species mass fractions. The discrete ordinate model was selected for the radiation and the k-ε model for the turbulence. The Enhanced Wall Treatment (EWT) model was chosen, which combines the two-layer model with enhanced wall functions and provides a y^+ insensitive near-wall treatment.

Non-premixed combustion with a steady diffusion flamelet and non-adiabatic energy treatment was selected for the species modelling. The Thermo file from the Ansys Model Fuel Library [40] was used as the thermodynamic database to create the flamelet. In addition, the GRI-Mech 3.0 [18] in Ansys Fluent was used to simulate the kinetics of the chemical reactions. This mechanism contains 325 reactions and 53 chemical species. This includes all reactants, products, and intermediate chemical species involved in the 325 reactions. As detailed in Section 3.2, this complex reaction mechanism model has been validated and accurately describes the reactions occurring during the combustion of the methane and hydrogen blends.

Regarding solver settings, SIMPLE (Semi-Implicit Method for Pressure-Linked Equations) was used for the numerical method. This algorithm is a widely used and robust numerical technique for solving equations. The PRESTO! (Pressure-Staggered Option) scheme, which is designed to provide accurate pressure values, is used. The numerical discretization methods are set to Second Order Upwind. This provides a precise approximation within the computational grid. In addition, the under-relaxation factors were used to stabilize the simulation.

Approximately 1500 iterations were performed until the convergence criteria were met. Monitoring the residuals over the iterations helps assess the simulation's convergence and accuracy. The convergence criteria for velocity, turbulence, and combustion were set to 10^{-3}, for radiation to 10^{-6}, and energy to 10^{-7}. The changes during the iterations must be close to zero, and the mass and energy balance must be close to zero.

5.3. Boundary Conditions

The boundary conditions at the inlet, outlet, and walls provide the necessary information to solve the equations. The model represents the internal volume of the furnace, where combustion and heat transfer occur. The inner walls of the furnace act as the crucible in contact with the molten material. Temperatures between 620 and 680 °C are required for melting magnesium in chamber die-casting. These varying temperatures influence the power consumption of the melting furnace [46] (pp. 561–562). For the model, a melting temperature of 680 °C and a heating power of 150 kW were chosen, reflecting real conditions during the melting process, as confirmed by the furnace manufacturers. The boundary conditions for the crucible walls were set to 953 K (680 °C), representing the temperature of the molten metal. The wall at the bottom of the furnace was set to 353 K (80 °C), based on data provided by furnace manufacturers. The external walls are exposed to ambient temperature. Therefore, the temperature of the outer walls, including the inlet and outlet, was assumed to be 303 K (30 °C). For each wall section, a specific heat transfer coefficient was calculated using the Nusselt correlation based on [47]. Table 4 provides an overview of the selected thermal conditions for each wall and the corresponding boundary conditions with their values.

Table 4. Walls boundary conditions for the simulations.

Wall Section	Thermal Conditions	Boundary Condition	Boundary Value
Crucible	Temperature	Temperature [K]	953
Furnace bottom wall	Temperature	Temperature [K]	353
Furnace external walls	Convection	Free Stream Temperature [K]	303
		Heat Transfer Coefficient [W/m^2 K]	7.4
Furnace top external walls	Convection	Free Stream Temperature [K]	303
		Heat Transfer Coefficient [W/m^2 K]	5
Inlet and Outlet Wall	Convection	Free Stream Temperature [K]	303
		Heat Transfer Coefficient [W/m^2 K]	7.4

The composition of the air and fuel mixture is predefined when the species model is selected for non-premixed combustion. Here, the different percentages of hydrogen in the fuel can be defined using the mole fraction as an input. With this information, the volumetric percentage (Vol-%) of hydrogen can be specified for the fuel mixture. To represent variations in hydrogen blending, four variants were defined with different Vol-% of hydrogen: 0%, 30%, 50%, and 70%. The model employs a single stream for air and fuel, with the fuel composition changing according to the mixture. This information is used to calculate each simulation's flamelets and the probability density function (PDF).

For all cases, the combustion power remained unchanged. Additionally, the geometry and cross-section of the inlet jets for air and fuel were kept constant. To calculate the boundary conditions for each variant, a constant air-fuel ratio of $\lambda = 1.1$ was assumed. A λ value of 1.1 implies a lean burn, which operates efficiently and results in lower emissions of CO and unburned hydrocarbons. With this information, along with the density of the gases and fixed parameters, the required velocity for air and fuel was calculated for different Vol-% of hydrogen. The inlet temperature and outlet pressure were maintained constant across all four variants. The selection of inlet velocity and outlet pressure as boundary conditions were made to enhance the numerical stability of the simulation. Table 5 shows the variation of the boundary conditions for the different hydrogen blends.

Table 5. Inlet and outlet boundary conditions for the simulations.

Boundary Condition		100 Vol.-% CH_4	70 Vol.-% CH_4 30 Vol.-% H_2	50 Vol.-% CH_4 50 Vol.-% H_2	30 Vol.-% CH_4 70 Vol.-% H_2
Inlet–Air	Velocity [m/s]	5819	5708	5595	5421
	Temperature [K]		303		
Inlet–Fuel	Velocity [m/s]	4869	6161	7484	9531
	Temperature [K]		323		
Outlet	Pressure [Pa]		0		

5.4. NO_x Post Processing

The pathways for thermal, prompt, and nitrous oxide (N_2O) simulations were selected to model NO_x. The composition of fuel and air was chosen from the list of species, primarily including hydrogen (H_2), methane (CH_4), oxygen (O_2), and nitrogen (N_2). The thermal NO_x was predicted using the instantaneous model, which offers well-defined species concentrations derived from combustion results. The fuel carbon number and equivalence ratio were entered to simulate the prompt parameters for each variant. The simulation of NO formation through an N_2O intermediate employed quasi-steady methods. The turbulence interaction mode was selected to incorporate turbulence effects, and the mixture fraction from the PDF was used to enhance the prediction of turbulence influences.

6. Simulation Results

In comparison to natural gas, hydrogen's combustion temperature exhibits higher temperatures. This increased temperature can potentially improve thermal efficiency but also presents challenges. The crucible material requires durability to withstand the increased thermal stresses induced by the elevated combustion temperatures. In addition, the higher temperatures of hydrogen combustion may lead to increased nitrogen oxide (NO_x) formation. The results of these simulations enable an evaluation of the combustion characteristics of hydrogen when blended with natural gas, including aspects such as thermal dynamics, combustion behaviour, and emissions output. This understanding contributes to the sustainable integration of hydrogen into existing natural gas infrastructures.

Figure 4 (left) illustrates the temperature distribution across four blending scenarios, each with varying hydrogen shares in the simulation models. The discretization of the model into finite volumes via a numerical grid enables the presentation of temperature values for each cell as a frequency distribution. The difference in temperature distribution between 30 Vol.-% hydrogen blending scenarios and 100% natural gas is minimal, indicating a similar distribution pattern across the cells. This minimal variance is quantified in Figure 4 (right), which shows a total temperature difference of 32 K between these two scenarios. Conversely, the temperature distribution difference between the 30% hydrogen blending scenarios and 50% hydrogen blending is the most pronounced, shifting towards higher temperatures and a total temperature difference of 75 K. As the proportion of hydrogen in the gas mixture increases, the changes become lower; the transition from 50% to 70% hydrogen blending results in a lower temperature difference of 30 K. These results demonstrate that the progression of temperature with varying hydrogen shares is not linear, with a marked change observable at a 30% hydrogen share. This finding is consistent with the literature cited in Section 3.3, indicating that up to 30% of hydrogen blends can be integrated without modifications into existing burners or technologies.

Hydrogen exhibits a superior specific heat capacity relative to methane or natural gas, leading to their mixture's higher overall specific heat capacity with increasing hydrogen shares. Adding hydrogen to methane also influences flame propagation; it also increases flame speed and modifies stability dynamics. Hydrogen's laminar flame speed exceeds methane's. Thereby, the blend's flame speed will increase with hydrogen's percentages.

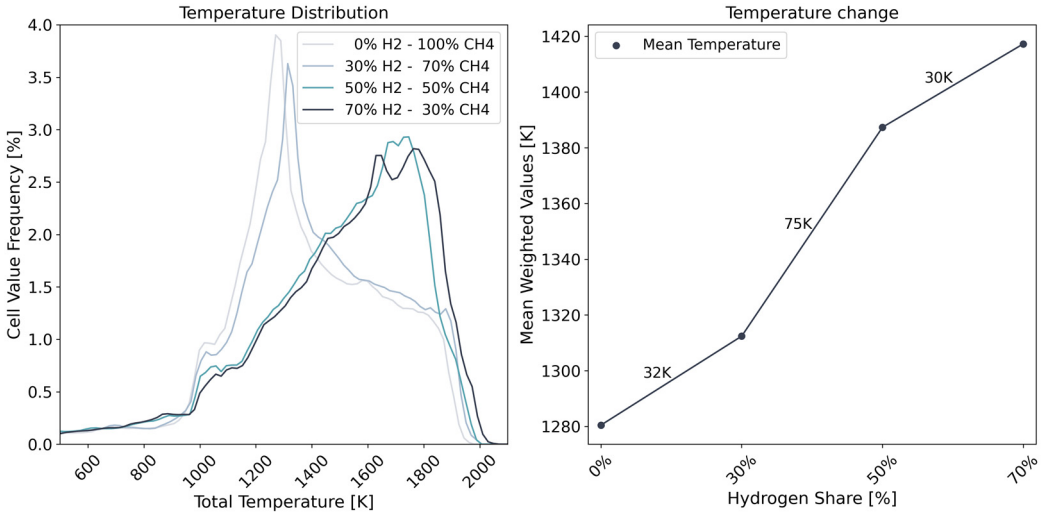

Figure 4. Temperature distribution and change of different hydrogen blending scenarios.

As shown in Figure 5, the comparative analysis of flame propagation under simulation scenarios of 70% hydrogen blending and a baseline of 100% methane reveals that the methane scenario has higher flame stability. The elevated flame velocity in the 70% hydrogen mixture scenario increases instability. This results in suboptimal mixing within the combustion chamber, which is noticeable due to the air steel that reaches the centre of the combustion chamber. Compared to methane combustion, 70% of hydrogen combustion has a different temperature distribution within the chamber and along the crucible walls and a different flame propagation and flammability. These changes can manifest in localised hotspots within the combustion chamber, highlighted within the simulation results by a red circle (Figure 5). These hotspots are critical areas of concern, as their presence can elevate NO_x formation and concentrations. An analysis of these findings emphasises the need to improve flame stability. With a burner redesign, a homogeneous heat distribution throughout the crucible can be achieved, facilitating the uniform melting of non-ferrous materials, which is required to maintain consistent product quality or process heat supply.

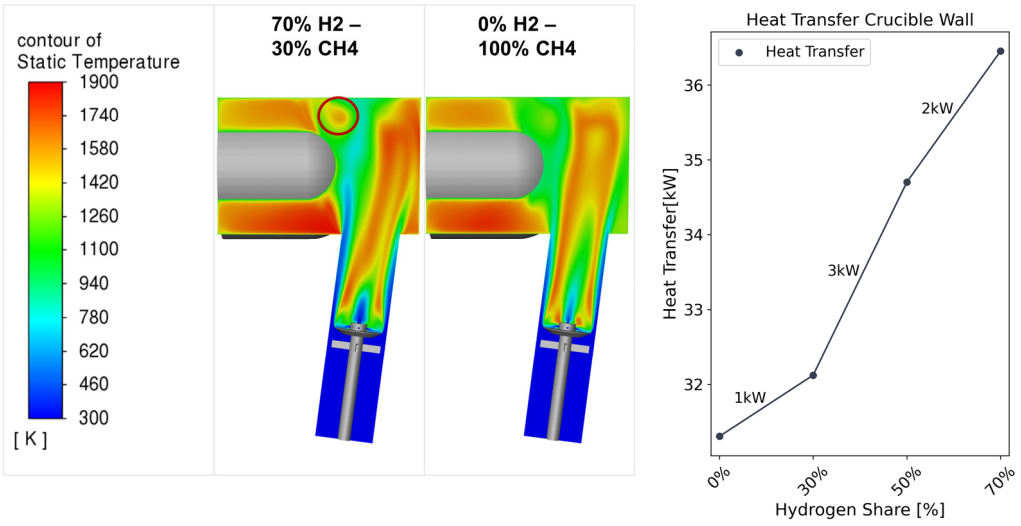

Figure 5. Temperature in the combustion chamber and heat transfer at the crucible wall.

Higher combustion temperatures, due to an increased hydrogen content in the fuel mixture, raise the thermal gradients at the furnace crucible wall while keeping the burner's power constant across all variants. This increased thermal gradient enhances both convective and radiative heat transfer from the furnace wall to the material inside, thus

accelerating the melting process. Figure 5 shows the increase of the heat transfer rate in kW for different hydrogen shares. The increased heat transfer efficiency is attributable to the superior thermal properties of hydrogen, including its higher thermal conductivity and heat capacity, which facilitate more effective energy transfer and distribution.

Another critical aspect is the development of emissions, estimated using post-processing techniques for combustions. All the variants maintain the same air-fuel ratio for lean combustion, ensuring that the combustion species from the air, namely oxygen and nitrogen, remain unchanged. The concentration of hydrogen and its temperature development primarily influence the intermediate formation of emissions. These emissions are simulated based on the assumptions described for modelling NOx formation in Section 4.3. Figure 6 illustrates the evolution of emissions for varying proportions of hydrogen mixed with natural gas. As expected, NO_x emissions increased with higher percentages of hydrogen due to elevated combustion temperatures. Using natural gas as a baseline, the NO_x emissions rise by 8% with a 30% hydrogen mixture, 26% with a 50% hydrogen mixture, and 41% with a 70% hydrogen mixture. Conversely, CO_2 emissions may decrease with a higher hydrogen content. Between 1 and 20% of CO_2 emissions can be reduced by using hydrogen blends compared to natural gas. Primarily, temperature increases influence the formation of NO_x. Therefore, mitigating the creation of different hot spots can significantly improve this process.

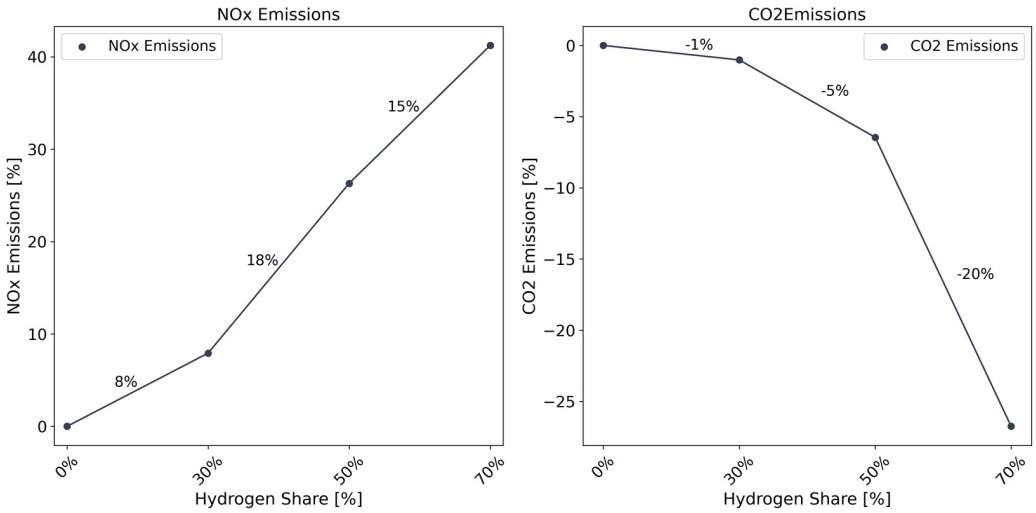

Figure 6. NO_x and CO_2 emissions development by different hydrogen blends.

Model Verification

To verify the simulation, the values obtained from the simulation are compared with the literature presented in Section 4.1. Specifically, the maximal and mean temperatures for the hydrogen blends and methane flames were analyzed. The results show that similar values are obtained within the range of the selected publications.

An observed temperature increase of about 11% was noted when the hydrogen share increased to 70% compared to the methane variant. This finding aligns with the study by Ilbas et al. [36], who conducted similar investigations. They compare the temperature levels during the combustion of a methane flame with a hydrogen share of 70 Vol-% and find that the temperature increases from approximately 2000 K for methane to 2210 K for the 70% hydrogen blend, also indicating an 11% increase.

Further comparisons with Bouziane et al. [33] indicate an even higher increase in the temperature of 56% for an 80% hydrogen blend compared to methane. Stefanizzi et al. [39] report a 5% increase for a 30% hydrogen blend compared to methane. The deviations from the presented results in this paper can be attributed to differences in numerical setups, boundary conditions, and the geometry of the burner or combustion chamber used.

7. Discussion and Conclusions

This paper investigates the combustion characteristics of hydrogen and methane/natural gas, with a focus on integrating hydrogen blends into natural gas for use in fired furnaces involved in melting processes. Using computational fluid dynamics (CFD) simulations, the study explores how changing the mixture of the fuel affects temperature profiles, heat transfer rates, and emissions within the furnace. The comparison was conducted for an identical firing power and the simulation focuses on a crucible furnace at a steady-state melting temperature of 680 °C. The simulation results provide a predictive framework for understanding how these changes might be applied to real furnaces.

A significant increase was noted in the combustion temperature when hydrogen constitutes more than 30 Vol.% of the fuel blend. This non-linear temperature rise, with a marked change observable at 30% hydrogen share, underscores the complexity of hydrogen integration. The results indicate a total mean temperature difference of 75 K between the 30 Vol.-% and 50 Vol.-% hydrogen scenarios. In contrast, the difference between 100% natural gas and a 30 Vol.% hydrogen blend is 32 K, and between 50 Vol.% and 70 Vol.% hydrogen blends, the difference is 30 K. This information highlights that the combustion behaviour changes at different hydrogen concentrations needed for optimizing hydrogen–natural gas blends.

Improvements in the heat transfer rate were also observed within the furnace crucible as hydrogen shares increased. This enhancement can be attributed to the superior thermal properties of hydrogen, such as higher thermal conductivity and heat capacity, which promote a more efficient energy transfer. Consequently, these properties could lead to better performance in industrial applications, such as die-casting melting furnaces, by facilitating faster and more uniform heating. The potential for CO_2 emissions reduction by integrating hydrogen into natural gas systems, which is needed to achieve lower carbon footprints for industrial processes, is observed in the results. The result of this work correlates with other findings in the literature. However, it extends the knowledge for a detailed application in die-casting furnaces at varying hydrogen shares, showing potential improvements in heat transfer efficiency and emissions reduction.

Future research on this topic can focus on hydrogen shares between 30 Vol.% and 50 Vol.% to further understand combustion changes since the most pronounced changes in combustion characteristics were observed there. Additionally, investigating air-fuel ratios for different hydrogen shares could improve the emissions, since adjusting the air-to-fuel mixture ratio, from stoichiometric to leaner mixtures, has the potential to decrease combustion temperatures and NO_x emissions.

Author Contributions: Conceptualization, L.J. and A.M.; methodology, L.J. and A.M.; software, L.J.; validation, L.J.; formal analysis, L.J.; investigation, L.J. and A.M.; resources, L.J.; data curation, L.J.; writing—original draft preparation, L.J.; writing—review and editing, L.J. and A.M.; visualization, L.J.; supervision, A.S.; project administration, A.M. All authors have read and agreed to the published version of the manuscript.

Funding: This research was conducted as part of the HyH2-Ofen Project (Autonomer, hybrider wasserstoffbetriebener Tiegelofen), and funded by InvestBW, Ministerium für Wirtschaft, Arbeit und Tourismus Baden-Württemberg [BW1_0176/02].

Data Availability Statement: All data and materials pertinent to this study are available upon request from the corresponding author. The data are not publicly accessible due to ongoing research activities involving a portion of the dataset.

Conflicts of Interest: The authors declare no conflicts of interest.

References

1. Die Bundesregierung. Klimaschutzgesetz und Klimaschutzprogramm. Available online: https://www.bundesregierung.de/breg-de/aktuelles/klimaschutzgesetz-2197410 (accessed on 23 June 2023).
2. BMWK—Bundesministerium für Wirtschaft und Klimaschutz. Gesamtausgabe der Energiedaten—Datensammlung des BMWK: Zhalen und Fakten: Energiedaten. Available online: https://www.bmwk.de/Redaktion/DE/Artikel/Energie/energiedaten-gesamtausgabe.html (accessed on 1 June 2023).
3. Universität Kassel. Das Potential Solarer Prozesswärme in Deutschland. Available online: https://www.uni-kassel.de/maschinenbau/institute/thermische-energietechnik/fachgebiete/solar-und-anlagentechnik/downloads (accessed on 1 June 2023).
4. Horng, P.; Kalis, M. Wasserstoff—Farbenlehre: Rechtwissenschaftliche und Rechtspolitische Kurzstudie. Available online: https://www.ikem.de/wp-content/uploads/2021/03/IKEM_Kurzstudie_Wasserstoff_Farbenlehre.pdf (accessed on 28 February 2023).
5. Linnemann, M.; Peltzer, J. *Wasserstoffwirtschaft Kompakt: Klimaschutz, Regulatorik und Perspektiven für Die Energiewirtschaft*; Springer Vieweg: Wiesbaden, Germany, 2022; ISBN 9783658390297.
6. Kurzweil, P. *Brennstoffzellentechnik: Grundlagen, Materialien, Anwendungen, Gaserzeugung*; 3., Überarbeitete und Aktualisierte Auflage; Springer Vieweg: Wiesbaden, Germany, 2016; ISBN 978-3-658-14934-5.
7. Stephan, W. Effiziente Energieverwendung in der Industrie: Effiziente Energienutzung in Nicht-Eisen-Metall Schmelzbetrieben. Available online: http://effguss.bdguss.de/?wpfb_dl=154 (accessed on 21 September 2022).
8. Umweltbundesamt. Stand der Technik der Österreichischen Gießereien: Gesetzliche Rahmenbedingungen, Technische Möglichkeiten und Gießereibetriebe in Österreich. Available online: https://www.umweltbundesamt.at/fileadmin/site/publikationen/REP0389.pdf (accessed on 31 August 2022).
9. Wünning, J.G. *Handbuch der Brennertechnik für Industrieöfen: Grundlagen—Brennertechniken—Anwendungen*, 3rd ed.; Vulkan-Verlag GmbH: Essen, Germany, 2019; ISBN 978-3-8027-3103-7.
10. Mickey, S.R.; Efficient Gas Heating of Industrial Furnaces. Thermal Processing Magazine, 20 January 2017. Available online: https://thermalprocessing.com/efficient-gas-heating-of-industrial-furnaces/ (accessed on 31 May 2024).
11. Bundesministerium für Bildung und Forschung BMBF. Kopernikus-Projekte: SynErgie: Bivalenter Schmelztiegelofen in Betrieb [Press Release]. 2023. Available online: https://www.kopernikus-projekte.de/aktuelles/news/synergie_bivalenter-schmelztiegelofen (accessed on 11 September 2023).
12. Köse, E.; Sauer, A. Reduction of energy costs and grid instability with energy flexible furnaces. *Procedia CIRP* **2018**, *72*, 832–838. [CrossRef]
13. Lee, S.-W.; Lee, H.-S.; Park, Y.-J.; Cho, Y.-S. Combustion and emission characteristics of HCNG in a constant volume chamber. *J. Mech. Sci. Technol.* **2011**, *25*, 489–494. [CrossRef]
14. Falfari, S.; Cazzoli, G.; Mariani, V.; Bianchi, G.M. Hydrogen Application as a Fuel in Internal Combustion Engines. *Energies* **2023**, *16*, 2545. [CrossRef]
15. Verhelst, S.; Demuynck, J.; Sierens, R.; Scarcelli, R.; Matthias, N.S.; Wallner, T. Update on the Progress of Hydrogen-Fueled Internal Combustion Engines. In *Renewable Hydrogen Technologies: Production, Purification, Storage, Applications and Safety*; Gandia, L.M., Arzamendi, G., Diéguez, P.M., Eds.; Elsevier Science: Amsterdam, The Netherlands, 2013; pp. 381–400, ISBN 9780444563521.
16. Undavalli, V.; Berwal, P.; Khandelwal, B. Chemical Kinetics of Hydrogen Combustion. In *Ammonia and Hydrogen for Green Energy Transition*, 1st ed.; Kumar, S., Agarwal, A.K., Khandelwal, B., Singh, P., Eds.; Springer Nature Singapore; Imprint Springer: Singapore, 2024; pp. 239–263, ISBN 978-981-97-0506-1.
17. Baulch, D.; Drysdale, D.; Horne, D.; Lloyd, A. (Eds.) *Evaluated Kinetic Data for High Temperature Reactions: Homogeneous Gas Phase Reactions of the H_2–N_2–O_2 System*; John Wiley & Sons, Ltd.: London, UK, 1973.
18. Smith, G.P.; Golden, D.M.; Frenklach, M.; Moriarty, N.W.; Eiteneer, B.; Goldenberg, M.; Bowman, C.T.; Hanson, R.K.; Song, S.; Gardiner, W.C., Jr.; et al. "GRI-Mech 3.0". 2008. Available online: http://combustion.berkeley.edu/gri-mech/version30/text30.html (accessed on 1 July 2024).
19. UC San Diego. The San Diego Mechanism: Chemical-Kinetic Mechanisms for Combustion Applications. 2014. Available online: https://web.eng.ucsd.edu/mae/groups/combustion/mechanism.html (accessed on 18 April 2024).
20. Ranzi, E.; Cavallotti, C.; Cuoci, A.; Frassoldati, A.; Pelucchi, M.; Faravelli, T. New reaction classes in the kinetic modeling of low temperature oxidation of n-alkanes. *Combust. Flame* **2015**, *162*, 1679–1691. [CrossRef]
21. Ranzi, E.; Frassoldati, A.; Grana, R.; Cuoci, A.; Faravelli, T.; Kelley, A.P.; Law, C.K. Hierarchical and comparative kinetic modeling of laminar flame speeds of hydrocarbon and oxygenated fuels. *Prog. Energy Combust. Sci.* **2012**, *38*, 468–501. [CrossRef]
22. Ranzi, E.; Frassoldati, A.; Stagni, A.; Pelucchi, M.; Cuoci, A.; Faravelli, T. Reduced Kinetic Schemes of Complex Reaction Systems: Fossil and Biomass-Derived Transportation Fuels. *Int. J. Chem. Kinet.* **2014**, *46*, 512–542. [CrossRef]
23. Shepherd, J.E. Explosion Dynamics Laboratory: Chemical Reaction and Thermodynamic Data. 2021. Available online: https://shepherd.caltech.edu/EDL/publicresources.html (accessed on 18 July 2024).
24. DVGW Deutscher Verein des Gas- und Wasserfaches e. V. *Erstmals 20 Prozent Wasserstoff im Deutschen Gasnetz: Innovationsprojekt von E.ON, Avacon und DVGW Startet Mit Wasserstoffbeimischungen*; DVGW Deutscher Verein des Gas- und Wasserfaches e. V: Bonn, Germany, 2021.
25. Chae, M.J.; Kim, J.H.; Moon, B.; Park, S.; Lee, Y.S. The present condition and outlook for hydrogen-natural gas blending technology. *Korean J. Chem. Eng.* **2022**, *39*, 251–262. [CrossRef]

26. Topolski, K.; Reznicek, E.; Erdener, B.; San Marchi, C.; Ronevich, J.; Fring, L.; Simmons, K.; Guerra Fernandez, O.; Hodge, B.; Chung, M. Hydrogen Blending into Natural Gas Pipeline Infrastructure: Review of the State of Technology: Technical Report. 2022. Available online: https://www.nrel.gov/docs/fy23osti/81704.pdf (accessed on 6 July 2024).
27. Fraunhofer Institute for Energy Economics and Energy System Technology. Limitations of Hydrogen Blending in the European Gas Grid: A Study on the Use, limitations and Cost of Hydrogen Blending in the European Gas Grid at the Transport and Distribution Level. Available online: https://www.iee.fraunhofer.de/content/dam/iee/energiesystemtechnik/en/documents/Studies-Reports/FINAL_FraunhoferIEE_ShortStudy_H2_Blending_EU_ECF_Jan22.pdf (accessed on 5 July 2023).
28. Ozturk, M.; Sorgulu, F.; Javani, N.; Dincer, I. An experimental study on the environmental impact of hydrogen and natural gas blend burning. *Chemosphere* **2023**, *329*, 138671. [CrossRef] [PubMed]
29. Ghaib, K. *Einführung in Die Numerische Strömungsmechanik*; Springer Vieweg: Wiesbaden, Germany, 2019; ISBN 9783658269234.
30. Ansys®. *Ansys Fluent Theory Guide*; ANSYS, Inc.: Canonsburg, PA, USA, 2019.
31. Laurien, E. *Numerische Strömungsmechanik: Grundgleichungen und Modelle—Lösungsmethoden—Qualität und Genauigkeit*; 4., Überarbeitete und Erweitere Auflage; Vieweg+Teubner: Wiesbaden, Germany, 2011; ISBN 9783834881212.
32. Ferziger, J.H. *Numerische Strömungsmechanik*; Springer: Berlin/Heidelberg, Germany, 2008; ISBN 9783540682288.
33. Bouziane, A.; Alami, A.; Zaitri, M.; Bouchame, B.; Bouchetara, M. Investigation of Swirl Stabilized CH_4 Air Flame with Varied Hydrogen Content by using Computational Fluid Dynamics (CFD) to Study the Temperature Field and Flame Shape. *Eng. Technol. Appl. Sci. Res.* **2021**, *11*, 6943–6948. [CrossRef]
34. Capurso, T.; Ceglie, V.; Fornarelli, F.; Torresi, M.; Camporeale, S.M. CFD analysis of the combustion in the BERL burner fueled with a hydrogen-natural gas mixture. *E3S Web Conf.* **2020**, *197*, 10002. [CrossRef]
35. Cellek, M.S.; Pınarbaşı, A. Investigations on performance and emission characteristics of an industrial low swirl burner while burning natural gas, methane, hydrogen-enriched natural gas and hydrogen as fuels. *Int. J. Hydrogen Energy* **2018**, *43*, 1194–1207. [CrossRef]
36. Ilbas, M.; Yılmaz, İ.; Veziroglu, T.N.; Kaplan, Y. Hydrogen as burner fuel: Modelling of hydrogen-hydrocarbon composite fuel combustion and NOx formation in a small burner. *Int. J. Energy Res.* **2005**, *29*, 973–990. [CrossRef]
37. Ilbas, M.; Yılmaz, İ.; Kaplan, Y. Investigations of hydrogen and hydrogen–hydrocarbon composite fuel combustion and NOx emission characteristics in a model combustor. *Int. J. Hydrogen Energy* **2005**, *30*, 1139–1147. [CrossRef]
38. Pashchenko, D. Hydrogen-rich fuel combustion in a swirling flame: CFD-modeling with experimental verification. *Int. J. Hydrogen Energy* **2020**, *45*, 19996–20003. [CrossRef]
39. Stefanizzi, M.; Stefanizzi, S.; Ceglie, V.; Capurso, T.; Torresi, M.; Camporeale, S.M. Analysis of the partially premixed combustion in a labscale swirl-stabilized burner fueled by a methane-hydrogen mixture. *E3S Web Conf.* **2021**, *312*, 11004. [CrossRef]
40. Ziani, L.; Chaker, A.; Chetehouna, K.; Malek, A.; Mahmah, B. Numerical simulations of non-premixed turbulent combustion of CH_4–H_2 mixtures using the PDF approach. *Int. J. Hydrogen Energy* **2013**, *38*, 8597–8603. [CrossRef]
41. Peters, N. Technische Verbrennung I: Institut für Technische Verbrennung. 2010. Available online: https://www.itv.rwth-aachen.de/fileadmin/LehreSeminar/TechnischeVerbrennung/Technische_Verbrennung_Diplom.pdf (accessed on 16 August 2023).
42. Joos, F. *Technische Verbrennung: Verbrennungstechnik, Verbrennungsmodellierung, Emissionen; Mit 65 Tabellen*; Springer: Berlin/Heidelberg, Germany, 2006; ISBN 978-3-540-34333-2.
43. Ansys®. *Ansys Fluent*; ANSYS, Inc.: Canonsburg, PA, USA, 2022.
44. Ansys®. *Ansys Fluent Users Guide*; ANSYS, Inc.: Canonsburg, PA, USA, 2019.
45. Ansys®. *Ansys SpaceClaim*; ANSYS, Inc.: Canonsburg, PA, USA, 2022.
46. Sauer, A.; Abele, E.; Buhl, H.U. (Eds.) *Energieflexibilität in der Deutschen Industrie: Ergebnisse aus dem Kopernikus-Projekt—Synchronisierte und Energieadaptive Produktionstechnik zur Flexiblen Ausrichtung von Industrieprozessen auf Eine Fluktuierende Energieversorgung (SynErgie)*; Fraunhofer: Stuttgart, Germany, 2019; ISBN 9783839614792.
47. Brenn, G. (Ed.) Heat Transfer. In *Analytical Solutions for Transport Processes: Fluid Mechanics, Heat and Mass Transfer*; Springer: Berlin/Heidelberg, Germany, 2017; pp. 189–237, ISBN 978-3-662-51421-4.